Small-signal dynamic model of a micro-grid including conventional and electronically interfaced distributed resources

F. Katiraei, M.R. Iravani and P.W. Lehn

Abstract: A systematic approach to small-signal modelling of a micro-grid system that includes conventional (rotating machine) and electronically interfaced distributed resource (DR) units is presented here. The proposed approach incorporates fundamental frequency deviations in the overall system model and provides a methodology for the analysis of autonomous micro-grid, which inherently is more prone to frequency changes than the conventional utility grid. The model represents (i) electro-mechanical dynamics of the synchronous machine including the exciter and the governor systems, (ii) dynamics of the voltage-sourced converter and its real/reactive power controllers and (iii) the network dynamics. The model is intended for the controller design/optimisation, evaluation of angle/voltage stability, investigation of torsional dynamics, controller interactions of electronically interfaced DR units and low-frequency power quality issues. Typical results from application of the proposed modelling approach to a study system are presented. The results are qualitatively verified on the basis of the comparison with those obtained from time-domain simulation in the PSCAD/EMTDC environment.

1 Introduction

Recent and ongoing technological, environmental, economical and social trends indicate proliferation of distributed resource (DR) units in the electric utility systems [1, 2], and have brought about the concept of a micro-grid [3–5]. A broad range of technical issues associated with the grid-connected and autonomous operational scenarios of a micro-grid system are presented in Piagi *et al.* [5] and Katiraei *et al.* [6].

Katiraei *et al.* [6] investigate micro-grid transients, on the basis of the digital time-domain simulation method, during and subsequent to an islanding process. Katiraei *et al.* [6] conclude that presence of electronically interfaced distributed generation (DG) units can effectively enhance power quality and maintain angle stability after islanding and during autonomous operation of the micro-grid. This is achieved by (i) exploiting the inherent fast and independent real and reactive power controllers of the electronically interfaced DG units and (ii) coordination of the controllers of various DG units.

Selection of controller parameters and control strategies for the case studies reported in Katiraei *et al.* [6] are based on a trial and error approach incorporating knowledge of the overall system characteristics. Selection of control/operational strategies, coordination of controls and optimisation of controller parameters on the basis of trial and error become a formidable task as the depth of DR penetration increases. Furthermore, trial and error approaches cannot reliably predict all micro-grid operational scenarios that can result in poor power quality or angle/voltage instability. Therefore a systematic approach to investigate micro-grid dynamics is required.

In a small-signal model of an interconnected power system, a large section of the system, with a good approximation, can usually be represented by an infinite bus and thus the base frequency is constant. In contrast, the base frequency of an autonomous micro-grid is subjected to excursions because of disturbances. The frequency deviation and its rate of change depend on the relative sizes and types of the DG units. The developed model captures frequency deviations of the micro-grid during autonomous mode of operation.

This paper presents a systematic approach and the mathematical formulations to develop a small-signal dynamic model of a micro-grid that includes the synchronous machine and the electronically interfaced DG unit. The system model includes the dynamic models of the lines and thus is a valid representation for the sub-synchronous frequency range. The develop model can be used to

- Design controllers of the micro-grid, for example governor and excitation systems of synchronous machine DG units, and real/reactive power controllers of electronically interfaced DG units.
- Optimise controller parameters of electronically interfaced DG units to take advantage of their fast responses in (i) enhancing voltage quality, (ii) controlling frequency and (iii) maintaining stability during and subsequent to a transition from one mode of operation to another.
- Identify operating points of DG units and control strategies that provide adequate stability margins to ensure sound transition between various modes of operation.
- Assist in developing appropriate operational strategies to accommodate various mixture of DG units and operational modes.

doi:10.1049/iet-gtd:20045207

Paper first received 9th October 2004 and in revised form 25th November 2005

The authors are with the Department of Electrical and Computer Engineering, University of Toronto, 10 King's College Road, Toronto, Ontario, Canada M5S 3G4

E-mail: f.katiraei@utoronto.ca

This paper also presents a frequency restoration strategy for the synchronous machine DG, through its governor, to return and maintain the system frequency to the original value during autonomous mode of operation. A phase-locked loop (PLL) system is used to dynamically lock the frequency of the electronically interfaced DG unit to that of the system.

A study system that includes two DG units, that is a synchronous machine and an electronically interfaced unit is adopted by Kaitraei *et al.* [6]. Operational modes and control strategies for the study system are described. The detail procedures and mathematical formulations to develop the small-signal dynamic model of the system during the autonomous micro-grid mode of operation are provided. Typical small-signal case studies are presented and various applications of the model are highlighted. The accuracy of the model is validated on the basis of the time-domain simulation of the system in the PSCAD/EMTDC environment. The procedures and mathematical formulations are presented in a general form in order that they can be expanded for a micro-grid with multiple DG units and loads and an arbitrary configuration.

2 Study system

Fig. 1 shows a single-line diagram of the system used to investigate dynamic performance of micro-grid controllers. The system is composed of a 13.8-kV, radial, three-feeder distribution subsystem, which is connected to the main grid through a 69-kV radial line. The main grid is represented as a 69-kV, 1000-MVA short-circuit capacity bus. The system parameters are given in Katiraei *et al.* [6].

The system includes two DG units, that is DG1 (5-MVA) and DG2 (2.5-MVA) on feeders $F1$ and $F3$, respectively. DG1 is a synchronous machine equipped with excitation and governor control systems. It may represent either a diesel-generator or a gas–turbine-generator unit. DG2 includes a voltage-sourced converter (VSC) to interface a prime source with the power system. DG2 represents a dispatchable source, for example (i) a micro-turbine generation unit, (ii) a fuel cell generation unit or (iii) a wind generation unit including battery storage. Thus, DG2 can supply real and reactive power to the system, within limits, on the basis of pre-specified control commands. DG2 provides control on its output real and reactive power components independently.

3 Modes of operation and control strategies

The 13.8-kV system of Fig. 1 has three distinct modes of operation: (i) the gridconnected mode, (ii) the autonomous micro-grid mode and (iii) the transition mode between the grid-connected and the autonomous micro-grid modes and vice versa.

- In the grid-connected mode

(i) The frequency is dictated by the main grid and DG1 and DG2 are synchronised with the system frequency.
(ii) Real power demand of the total load is met by the main grid, DG1 and DG2. The levels of contribution of DG1 and DG2 are usually determined on the basis of the economics of the case. Thus, changes in the load are compensated by the grid.
(iii) Voltage profile requirements and reactive power demands are met by the main grid, DG1, DG2 and other reactive power sources, for example the fixed, shunt capacitor at the 13.8-kV bus (Fig. 1). Reactive power outputs of DG1 and DG2 are dynamically adjusted on the basis of the voltage profile constraints.

- In the autonomous micro-grid mode of operation

(i) Frequency of the 13.8-kV system must be maintained by DG1 and DG2. After separation from the main grid, frequency variations and the rate of frequency variation of the autonomous micro-grid depend on the power balance condition. If the total generation of DG1 + DG2

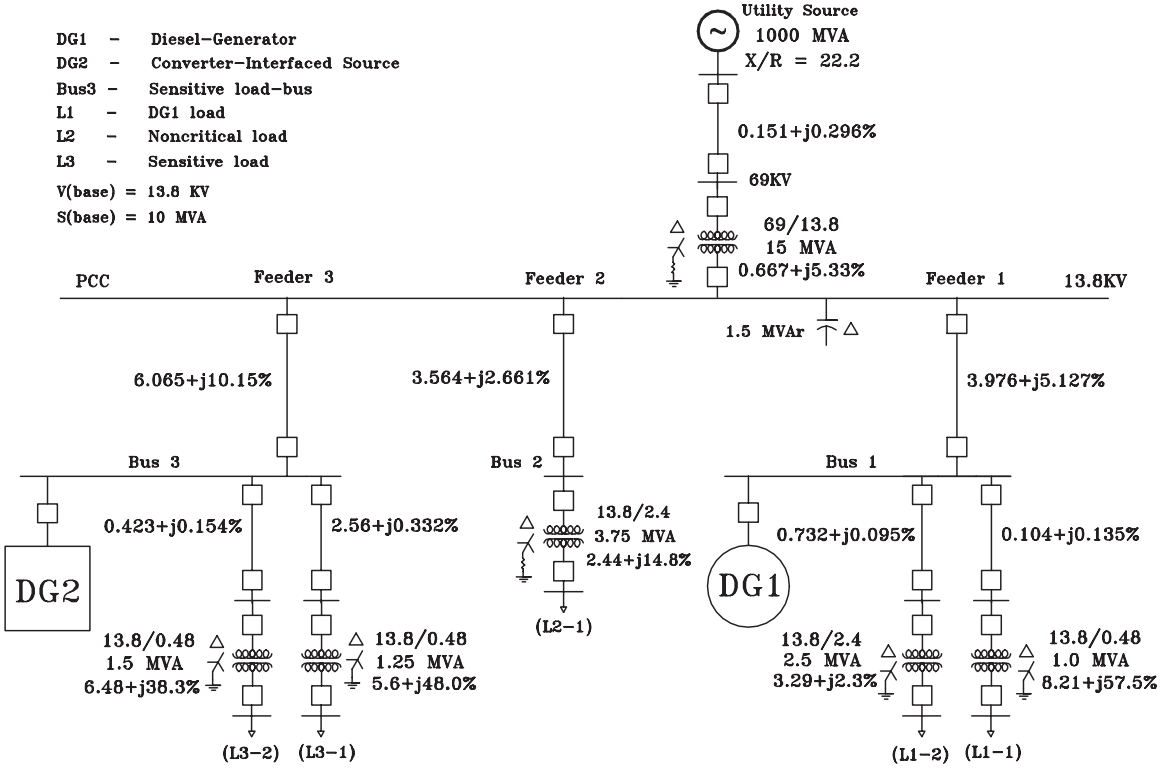

Fig. 1 *Single-line diagram of the study system*

prior to islanding is less (greater) than the micro-grid load demands, formation of the autonomous micro-grid results in reduction (rise) in the frequency. Employing an adequately fast-response, realpower balancing strategy between the DG units will compensate the load demand and return the system frequency to the specified range of 57–60.5 Hz [7] during transients. Furthermore, frequency restoration is applied to adjust the frequency to the standard utility operation range of 59.3–60.5 Hz, through balancing the power generation set-points of DG1 and DG2, during steady-state operation [8].

(ii) The total real power demand is provided by DG1 and DG2. Since DG2 is coupled to the micro-grid through power electronics, it can respond to the load dynamics faster than DG1, and thus it can effectively maintain frequency and enhance angle stability. Adequate real power margin for DG2 must be available to take advantage of its fast response during the micro-grid dynamics. The instantaneous real power from DG2 can be adjusted by controlling real power component of its converter current, using a current-controlled VSC. Implementing the current controller in the $dq0$ frame [9], the output real power of the unit is determined by the d-axis current of the converter.

(iii) Reactive power demand of the total load and voltage profile is provided by DG1, DG2 and reactive power sources, for example shunt capacitors. The capability of DG2 to rapidly respond to its output-power and terminal voltage make it the prime candidate to dynamically control the micro-grid reactive power. This suggests that an adequate margin in the output reactive power of DG2 must be available to meet reactive power demand of the micro-grid dynamically. The reactive power is controlled through the q-component of the converter current [9].

- In the transition mode, depending on the real- and reactive-power control strategies of the pre- and post-transition modes, there might be a need either to switch from one set of controllers to another set or change the controller parameters, particularly for DG2 [6]. Thus, controls of the grid-connected and autonomous micro-grid modes must be coordinated to assure successful transition from one mode to the other. The micro-grid may be equipped with discrete control/protection strategies to assist the system performance during the transition mode. Such strategies are dependent on the system configuration, transient characteristics and anticipated transient durations. These issues are not discussed in this paper.

4 Mathematical model of micro-grid

Fig. 2 shows a single-line diagram of the 13.8-kV distribution system of Fig. 1 during an autonomous micro-grid mode of operation. To investigate the dynamic behaviour of the autonomous micro-grid, including the controller of DG1 and DG2, a linearised mathematical model of the micro-grid in the general form of

$$\Delta\dot{\boldsymbol{x}} = A\Delta\boldsymbol{x} + B\Delta\boldsymbol{u} \tag{1}$$

is developed. To construct (1), the ordinary differential equations (ODEs) representing (i) DG1 and its excitation and governor, (ii) DG2 and its real/reactive/voltage controls and (iii) the network including the loads and the fixed capacitor banks, are developed in their respective local $dq0$ reference frames. Then, the developed equations are transformed to the micro-grid global $dq0$ frame, linearised about an operating point and arranged in the state-space form of (1). Since a three-phase, balanced system is assumed, 0-axis components are zero and are not discussed any further.

In the micro-grid system of Fig. 2, the global reference frame is defined on Bus-1, that is at the terminal of DG1. Fig. 3 identifies the global rotating reference frame of the micro-grid by a d- and q-axis rotating at the angular frequency of ω_e. The d-axis is in the direction of the voltage space vector of Bus-1, $\boldsymbol{v}^{G1}$.

The local reference frame of DG1 is depicted on Fig. 3 by $d1$- and $q1$-axis rotating at dynamic speed ω_r. This reference frame is locked to the rotor of DG1 [10]. Under steady-state conditions, $q1$-axis is in the direction of the machine internal voltage E_g (Fig. 3). Angle δ_0, between d-axis and $q1$-axis of Fig. 3, is the power angle of DG1 and

$$\delta_0 = \frac{\pi}{2} + \delta_1 \tag{2}$$

where δ_1 is the instantaneous rotor angle of DG1 in its local reference frame with the initial phase angle difference of δ_1^0 between global d–q frame and the local $d1$–$q1$ reference frame.

The local rotating reference frame of DG2 is defined by $d2$-axis and $q2$-axis (Fig. 3) where $d2$-axis is in the direction of the voltage space vector at Bus-3, $\boldsymbol{v}^{G2}$. The $d2$–$q2$ frame rotates at dynamic speed ω_s of $\boldsymbol{v}^{G2}$. The instantaneous phase angle of $\boldsymbol{v}^{G2}$ is represented by δ_2 with the initial phase angle difference between the global d–q reference frame and the $d2$–$q2$ reference frame given by δ_2^0 (Fig. 3).

The rotating speed of the global reference frame, that is ω_e, is not necessarily a constant speed. Thus, subsequent to disconnection from the main grid, it may deviate from

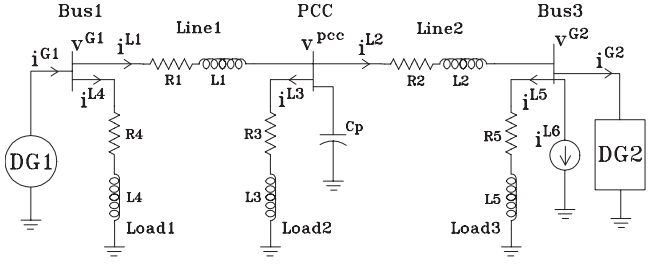

Fig. 2 *Single-line diagram of the micro-grid used for small-signal analysis*

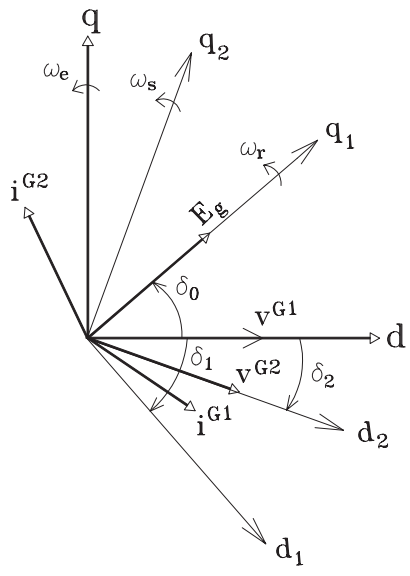

Fig. 3 *Global and local rotating reference frames of the study system of Fig. 2*

the synchronous value. However, the frequency control, imposed by the governor system of DG1 and the frequency restoration control of DG2, brings ω_e back to the synchronous speed under steady-state operating conditions. The frequency controls also synchronise angular frequencies of the rotating reference frames of DG1 (ω_r) and DG2 (ω_s) with the speed of the global reference frame (ω_e). However, impacts of those variations are reflected on the phase–angle differences between the $d1-q1$ axes of DG1 and the $d-q$ axes of the global reference frame, also between the $d2-q2$ axes of DG2 and the $d-q$ axes of the global reference frame [11].

To construct (1), the equations of each subsystem n, that is DG1 and DG2 subsystems, are first transformed to the global $d-q$ frame based on [10]

$$\boldsymbol{f}^g = \boldsymbol{T}_n \boldsymbol{f}^n \tag{3}$$

where $\boldsymbol{f}^g = [\boldsymbol{f}_q^g \quad \boldsymbol{f}_d^g]^{\mathrm{T}}$ is the vector of components of variable $\boldsymbol{f}$ in the global $d-q$ frame, $\boldsymbol{f}^n = [\boldsymbol{f}_q^n \quad \boldsymbol{f}_d^n]^{\mathrm{T}}$ is the vector of components of variable $\boldsymbol{f}$ in the nth subsystem $dn-qn$ frame. Transformation matrix $\boldsymbol{T}_n$ is [10]

$$\boldsymbol{T}_n = \begin{bmatrix} \cos\delta_n & \sin\delta_n \\ -\sin\delta_n & \cos\delta_n \end{bmatrix} \tag{4}$$

δ_n is the angle between the d-axis of the global reference frame and the d-axis of the nth subsystem reference frame. Then, the transformed equations are linearised about an operating point and combined in the general state-space form of (1). A systematic procedure to develop (1) from the overall system equations is described in Parniani [12] and Undrill [13].

4.1 Dynamic model of DG1

DG1 is a two-pole, three-phase synchronous machine, equipped with excitation and governor systems. The rotor electrical system of DG1 is represented by two windings on each axis. The dynamic of the electrical system of DG1, in its rotor reference frame [10], which is identified by $d1-q1$ in Fig. 3, is given by

$$v = Ei + F\frac{\mathrm{d}}{\mathrm{d}t}(i) \tag{5}$$

where

$$\boldsymbol{v} = \begin{bmatrix} \boldsymbol{v}_{q1} & \boldsymbol{v}_{d1} & \boldsymbol{v}_{k1q1} & \boldsymbol{v}_{k2q1} & \boldsymbol{v}_{kd1} & \boldsymbol{v}_{fd1} \end{bmatrix}^{\mathrm{T}}$$

$$\boldsymbol{i} = \begin{bmatrix} \boldsymbol{i}_{q1} & \boldsymbol{i}_{d1} & \boldsymbol{i}_{k1q1} & \boldsymbol{i}_{k2q1} & \boldsymbol{i}_{kd1} & \boldsymbol{i}_{fd1} \end{bmatrix}^{\mathrm{T}}$$

are vectors of voltages and currents of the stator windings ($d1$, $q1$), damper windings ($k1q1$, $k2q1$, $kd1$) and field winding ($fd1$). Matrices $\boldsymbol{E}$ and $\boldsymbol{F}$ are given in Krause [10].

The rotating mechanical system of DG1 is represented by an equivalent single, rigid mass. The dynamic model of the rotating mass is given by

$$J\frac{\mathrm{d}^2}{\mathrm{d}t^2}(\delta 1) + D\frac{\mathrm{d}}{\mathrm{d}t}(\delta_1) = T_{\mathrm{m}} - T_{\mathrm{e}} \tag{6}$$

where J and D are the inertia and damping constants, respectively. Angle δ_1 is defined by (2). T_{m} and T_{e} are the mechanical and the air-gap torques, respectively [10] and

$$T_{\mathrm{e}} = \frac{3}{2\omega_r}(\boldsymbol{v}_{q1}\boldsymbol{i}_{q1} + \boldsymbol{v}_{d1}\boldsymbol{i}_{d1}) \tag{7}$$

The excitation and governor systems of DG1 are represented by a generic dc excitation system adopted from IEEE WG [14], and the IEEE governor model on the basis of the speed-droop characteristic adopted from IEEE WG [15], respectively.

A state-space model of DG1, in its rotor reference frame of $d1-q1$, is obtained by combining dynamic models of the electrical system (5), the mechanical system (6) and the governor/excitation controls. The model is then transformed to the micro-grid global $d-q$ frame, and linearised as given by

$$\Delta\dot{\boldsymbol{x}}_{G1} = \boldsymbol{A}_{G1}\Delta\boldsymbol{x}_{G1} + \boldsymbol{B}_{G1}^{v}\Delta\boldsymbol{v}^{G1} + \boldsymbol{B}_{G1}^{u}\Delta\boldsymbol{u}_{G1} \tag{8}$$

where

$$\Delta\boldsymbol{x}_{G1} = \begin{bmatrix} \Delta\boldsymbol{i}_q^{G1} & \Delta\boldsymbol{i}_d^{G1} & \Delta\boldsymbol{i}_{k1q1} & \Delta\boldsymbol{i}_{k2q1} & \Delta\boldsymbol{i}_{kd1} & \Delta\boldsymbol{i}_{fd1} & \Delta\dot{\boldsymbol{\delta}}_1 & \Delta\boldsymbol{\delta}_1 \end{bmatrix}^{\mathrm{T}}$$

is the vector of state variables of DG1 in which $\Delta\boldsymbol{i}_q^{G1}$ and $\Delta\boldsymbol{i}_d^{G1}$ are the current components of the stator windings in the global reference frame. In (8)

$$\Delta\boldsymbol{v}^{G1} = \begin{bmatrix} \Delta\boldsymbol{v}_q^{G1} & \Delta\boldsymbol{v}_d^{G1} \end{bmatrix}^{\mathrm{T}}$$

is the voltage vector representing the transformed and linearised stator voltages in the global $d-q$ frame, and

$$\Delta\boldsymbol{u}_{G1} = \begin{bmatrix} \Delta\boldsymbol{v}_{fd1} & \Delta T_{\mathrm{m}} \end{bmatrix}^{\mathrm{T}}$$

is the vector of input control signals $\Delta\boldsymbol{v}_{fd1}$ and ΔT_{m} provided by the excitation system and the governor, respectively. The state matrix $\boldsymbol{A}_{G1}$, voltage coefficient matrix $\boldsymbol{B}_{G1}^{v}$ and matrix of gain factors for the input control signals, $\boldsymbol{B}_{G1}^{u}$, can also be found in Krause [10].

4.2 Dynamic model of DG2

DG2 is composed of two subsystems (i) the converter power circuit and (ii) the converter controls. Fig. 4 shows a schematic diagram of DG2 in which the power circuit and the control subsystems are identified.

4.2.1 Power circuit: The power circuit of DG2 is shown in Fig. 4 comprising a DC/AC converter and interconnection impedances. The dc-side of the converter is represented by a constant, unidirectional voltage V_{dc}. Each phase of the

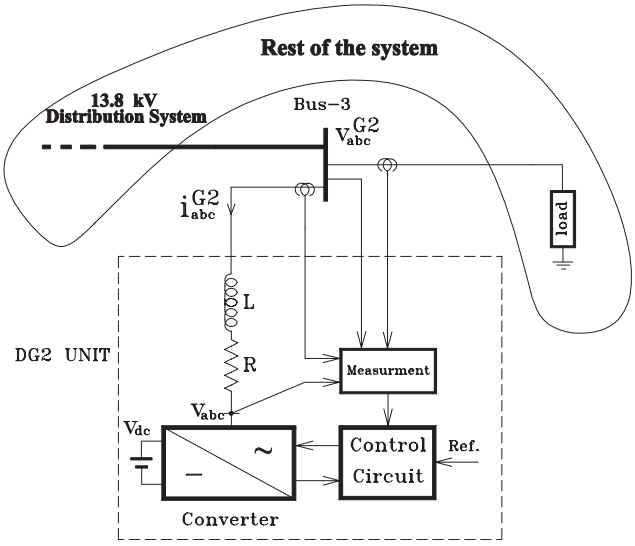

Fig. 4 *Electronically interfaced DG2 unit*

ac-side is represented by series connected R and L elements. R includes the on-state switch resistances, resistance of the series ac-side filter and the resistance of the interface transformer. L represents the inductance of the series filter and the leakage of the interface transformer. The dynamic model of the power circuit, in the ac-side abc frame, is obtained from the ODEs of the three phases as

$$\boldsymbol{v}_{abc} = -R\boldsymbol{i}^{G2}_{abc} - L\frac{\mathrm{d}}{\mathrm{d}t}(\boldsymbol{i}^{G2}_{abc}) + \boldsymbol{v}^{G2}_{abc} \tag{9}$$

where $\boldsymbol{v}_{abc}$, $\boldsymbol{v}^{G2}_{abc}$ and $\boldsymbol{i}^{G2}_{abc}$ are vectors of the instantaneous values of the converter output voltages, bus voltages and the converter output currents, respectively (Fig. 4). Then (9) is transformed to the local rotating reference frame of DG2, that is $d2-q2$, which is defined at Bus-3 (Fig. 2). This reference frame is specified by $d2-q2$ in Fig. 3 and rotates at frequency ω_s corresponding to the speed of the voltage space vector of Bus-3 [9]. The transformed equations in the $d2-q2$ reference frame are

$$\frac{\mathrm{d}}{\mathrm{d}t}(\boldsymbol{i}^{G2}) = \begin{bmatrix} \dfrac{-R}{L} & -\omega_s \\ \omega_s & \dfrac{-R}{L} \end{bmatrix} \boldsymbol{i}^{G2} + \frac{1}{L}(\boldsymbol{v}^{G2} - v) \tag{10}$$

where

$$\boldsymbol{i}^{G2} = \begin{bmatrix} \boldsymbol{i}^{G2}_{q2} & \boldsymbol{i}^{G2}_{d2} \end{bmatrix}^{\mathrm{T}}, \boldsymbol{v}^{G2} = \begin{bmatrix} \boldsymbol{v}^{G2}_{q2} & \boldsymbol{v}^{G2}_{d2} \end{bmatrix}^{\mathrm{T}}, \boldsymbol{v} = \begin{bmatrix} \boldsymbol{v}_{q2} & \boldsymbol{v}_{d2} \end{bmatrix}^{\mathrm{T}}$$

In this study, the dc-side is assumed as an ideal source and represented by a fixed voltage. Thus, it introduces no dynamic in the converter model. This fixed voltage is a representation of the prime source and/or energy storage. If the net dc-side is not represented as an ideal source, its dynamic can be represented as part of the converter circuit and included as part of the overall system model [9].

4.2.2 Controls: The output real power and terminal voltage of DG2 are controlled by the instantaneous values of the converter output current components $\boldsymbol{i}^{G2}_{d2}$ and $\boldsymbol{i}^{G2}_{q2}$, respectively [9]. Fig. 5*a* shows a block diagram of the control system of DG2. The control system includes (i) two internal current loops to control the converter current components $\boldsymbol{i}^{G2}_{d2}$ and $\boldsymbol{i}^{G2}_{q2}$ and (ii) two external control loops, which generate the reference values for the internal loops on the basis of the desired real power and voltage at the converter terminal. Input signals for the $d2-q2$ current control block (Fig. 5*a*) are $\boldsymbol{i}^{G2}_{d2}$ and $\boldsymbol{i}^{G2}_{q2}$ of DG2 currents passed through two low-pass filters (LPF) block of Fig. 5*a*. The filter time constants are in the range of 2–4 ms. In practice, LPF is employed to filter out converter switching harmonics and noises.

The output signals of the $d2-q2$ current control block are the reference voltages of DG2. Fig. 5*b* shows the signal processing block of the control system. This includes a PLL [16] to estimate phase angle, δ_2, of the voltage vector of Bus-3 in the space of rotational frame and to identify the reference frame for the instantaneous real/reactive power calculator. The conventional PLL is composed of a voltage control oscillator to monitor the input signal and a loop filter to follow variations in the angular frequency of the input signal. The PLL model is explained in Appendix A [16].

The real power controller of Fig. 5*a* determines $\boldsymbol{i}_{d2}$(ref) on the basis of instantaneous value of real power output of the converter $P_{\mathrm{out}}(t)$ and the specified power set-point P_{ref}. It consists of a proportional integral (PI) controller and a limiter. The design criteria for the real power controller are

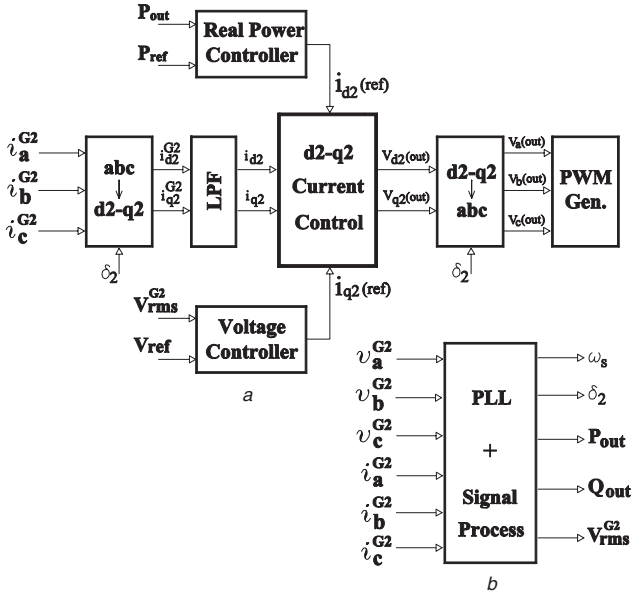

Fig. 5 *Control block diagram for DG2 unit*

a $d2-q2$ current control and interface blocks
b Signal processing block

to meet the power demand of the system during transients. Thus as part of the real power control strategy, the limit on the d-component of the current is increased up to the maximum permissible converter current to supply the transient real power requirements and support short time scale power balance of the system [11]. The time constant and gain of the real power controller are determined on the basis of the overshoot, for example $<20\%$, and response time, for example ~ 20 ms. The controller parameters are optimised according to the range of variations given by sensitivity analysis of the eigenvalues of the control system.

The voltage controller of Fig. 5*a* determines $\boldsymbol{i}_{q2}$(ref) to achieve bus voltage regulation within the pre-specified limits [7]. The error signal between the measured rms value of bus voltages V^{G2}_{rms} and the reference V_{ref} is fed to a PI controller. The output of the PI controller is $\boldsymbol{i}_{q2}$(ref). Between the $d2$-axis and the $q2$-axis current controllers, the control priority is given to the $d2$-axis by limiting $\boldsymbol{i}_{q2}$(ref) signal to the difference between the maximum converter current and $\boldsymbol{i}_{d2}$(ref), subsequent to an islanding process. Thus real-power control is the priority for DG2.

The model of (10) indicates that current components $[\boldsymbol{i}^{G2}_{q2} \quad \boldsymbol{i}^{G2}_{d2}]^{\mathrm{T}}$ are coupled through $-\omega_s \boldsymbol{i}^{G2}_{d2}$ and $\omega_s \boldsymbol{i}^{G2}_{q2}$ terms. The coupling is eliminated [9] by introducing new variables $\boldsymbol{v}'_{d2}$ and $\boldsymbol{v}'_{q2}$ as given by

$$\boldsymbol{v}' = \boldsymbol{v}^{G2} - \boldsymbol{v} + (\omega_s L)[-\boldsymbol{i}^{G2}_{d2} \quad \boldsymbol{i}^{G2}_{q2}]^{\mathrm{T}} \tag{11}$$

where $\boldsymbol{v}' = [\boldsymbol{v}'_{q2} \quad \boldsymbol{v}'_{d2}]^{\mathrm{T}}$. Substituting for $\boldsymbol{v}$ from (11) in (10) yields

$$\frac{\mathrm{d}}{\mathrm{d}t}(\boldsymbol{i}^{G2}) = -\frac{R}{L}\boldsymbol{i}^{G2} + \frac{1}{L}\boldsymbol{v}' \tag{12}$$

Equation (12) represents decoupled $\boldsymbol{i}^{G2}_{d2}$ and $\boldsymbol{i}^{G2}_{q2}$ currents. Fig. 6 shows decoupled current controllers, which are illustrated in the $d2-q2$ current control block of Fig. 5*a*.

The state-space model of the converter of DG2 is constructed first by transforming (12) to the global $d-q$ frame on the basis of (3), and then linearising the transformed equations about the operating point [11]. The linearised state-space model of DG2 is

$$\Delta\dot{\boldsymbol{x}}_{G2} = \boldsymbol{A}_{G2}\Delta\boldsymbol{x}_{G2} + \boldsymbol{B}^{v'}_{G2}\Delta\boldsymbol{v}' + \boldsymbol{B}^{v}_{G2}\Delta\boldsymbol{v}^{G2} + \boldsymbol{B}^{\omega}_{G2}\Delta\boldsymbol{\omega}_s \tag{13}$$

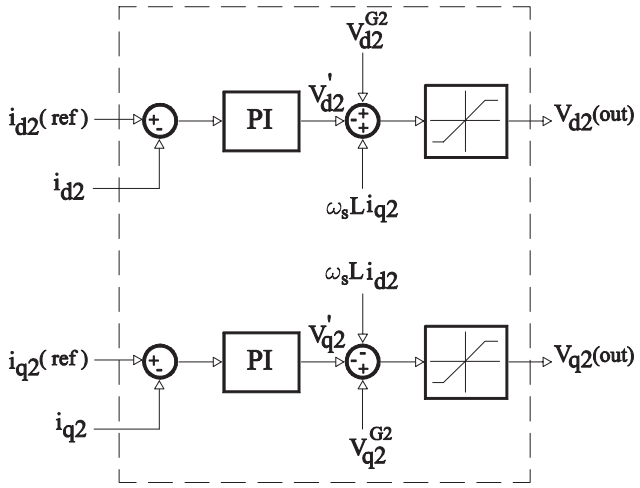

Fig. 6 *DG2 current controllers for d- and q-axis*

where

$$\Delta \boldsymbol{x}_{G2} = \begin{bmatrix} \Delta \boldsymbol{i}_q^{G2} & \Delta \boldsymbol{i}_d^{G2} \end{bmatrix}^{\mathrm{T}}, \quad \Delta \boldsymbol{v}' = \begin{bmatrix} \Delta \boldsymbol{v}'_q & \Delta \boldsymbol{v}'_d \end{bmatrix}^{\mathrm{T}}$$

and $\Delta\omega_s$ is the deviation in rotational speed of $d2-q2$ frame, (Fig. 3). Matrices $\boldsymbol{A}_{G2}$, $\boldsymbol{B}_{G2}^{v'}$, $\boldsymbol{B}_{G2}^{v}$ and $\boldsymbol{B}_{G2}^{\omega}$ in (13) are defined as follow

$$\boldsymbol{A}_{G2} = \boldsymbol{T}_2^{-1}\boldsymbol{A}_{q2d2}\boldsymbol{T}_2, \quad \boldsymbol{B}_{G2}^{v'} = \boldsymbol{T}_2^{-1}\boldsymbol{B}_{q2d2}^{v}$$

$$\boldsymbol{B}_{G2}^{v} = \boldsymbol{T}_2^{-1}\boldsymbol{A}_{q2d2}\boldsymbol{I}_{\delta 2}\boldsymbol{M}_{qd}, \boldsymbol{B}_{G2}^{\omega} = -\boldsymbol{T}_2^{-1}\boldsymbol{I}_{\delta_2}$$

where

$$\boldsymbol{A}_{q2d2} = \mathrm{diag}\begin{bmatrix} -\dfrac{R}{L} & -\dfrac{R}{L} \end{bmatrix}, \quad \boldsymbol{B}_{q2d2}^{v} = \mathrm{diag}\begin{bmatrix} \dfrac{1}{L} & \dfrac{1}{L} \end{bmatrix}$$

$$\boldsymbol{I}_{\delta_2} = \begin{bmatrix} \boldsymbol{i}_d^{oG2} & -\boldsymbol{i}_q^{oG2} \end{bmatrix}^{\mathrm{T}},$$

$$\boldsymbol{M}_{qd} = \begin{bmatrix} \dfrac{\boldsymbol{v}_d^{oG2}}{\boldsymbol{v}_d^{oG2^2} + \boldsymbol{v}_q^{oG2^2}} & \dfrac{-\boldsymbol{v}_q^{oG2}}{\boldsymbol{v}_d^{oG2^2} + \boldsymbol{v}_q^{oG2^2}} \end{bmatrix}^{\mathrm{T}}$$

transformation matrix $\boldsymbol{T}_2$ is given by (4).

The dynamic model of the control system of DG2, Figs. 5 and 6, is developed in the $d2-q2$ reference using the linearised procedure and model development procedure discussed in Appendix A and also further discussed in Katiraci [11]. The state-space representation of the control system of DG2 is

$$\Delta \dot{\boldsymbol{x}}_c = \boldsymbol{A}_c \Delta \boldsymbol{x}_c + \boldsymbol{C}_{G2}\Delta \boldsymbol{x}_{G2} + \boldsymbol{C}_{G2}^{v}\Delta \boldsymbol{v}^{G2} + \boldsymbol{C}^{v}\Delta \boldsymbol{v} + \boldsymbol{C}_{G2}^{u}\Delta \boldsymbol{u}_{G2} \tag{14}$$

where

$$\Delta \boldsymbol{x}_c = \begin{bmatrix} \Delta \boldsymbol{v}_{q2'}^{G2} & \Delta \boldsymbol{v}_{d2'}^{G2} & \Delta \boldsymbol{v}_{q2'} & \Delta \boldsymbol{v}_{d2'} & \Delta \boldsymbol{i}_{iq2} & \Delta \boldsymbol{i}_{id2} & \Delta \boldsymbol{i}_{q2'}^{G2} \\ \Delta \boldsymbol{i}_{d2'}^{G2} & \Delta \boldsymbol{v}_{iq2} & \Delta \boldsymbol{v}_{id2} & \Delta \omega_s \end{bmatrix}^{\mathrm{T}}$$

$$\Delta \boldsymbol{v}^{G2} = \begin{bmatrix} \Delta \boldsymbol{v}_{q2}^{G2} & \Delta \boldsymbol{v}_{d2}^{G2} \end{bmatrix}^{\mathrm{T}}, \Delta \boldsymbol{v} = [\Delta \boldsymbol{v}_{q2} \quad \Delta \boldsymbol{v}_{d2}]^{\mathrm{T}}$$

$$\Delta \boldsymbol{u}_{G2} = [\Delta \boldsymbol{P}_{\mathrm{ref}} \quad \Delta \boldsymbol{V}_{\mathrm{rms}}]^{\mathrm{T}}$$

The detailed definition of coefficient matrices in (14) is given in Katiraei [11].

The method for selecting an independent set of state variables to fully represent the control system of DG2 is described in Appendix A.

4.3 Dynamic model of the network

Fig. 2 shows a one-line diagram of the network. The lines and the constant loads are represented by series-connected RL branches in each phase and, where applicable, are lumped together. The fixed capacitor bank at the substation bus is modelled by an equivalent shunt capacitor, C_p, in each phase.

The nonlinear part of the load at Bus-3 [6] (Fig. 1) is represented by an equivalent current source at the fundamental frequency in Fig. 2. The dynamic model of the network is represented by the three-phase ODEs of the RL branches and shunt capacitor branch in the *abc* reference frame as

$$\begin{aligned} R_1 \boldsymbol{i}^{L1} + L_1 \frac{\mathrm{d}}{\mathrm{d}t}(\boldsymbol{i}^{L1}) &= \boldsymbol{v}^{G1} - \boldsymbol{v}^{\mathrm{pcc}} \\ R_2 \boldsymbol{i}^{L2} + L_2 \frac{\mathrm{d}}{\mathrm{d}t}(\boldsymbol{i}^{L2}) &= \boldsymbol{v}^{\mathrm{pcc}} - \boldsymbol{v}^{G2} \\ C_p \frac{\mathrm{d}}{\mathrm{d}t}(\boldsymbol{u}^{\mathrm{pcc}}) &= \boldsymbol{i}^{L1} - \boldsymbol{i}^{L2} - \boldsymbol{i}^{L3} \end{aligned} \tag{15}$$

where $\boldsymbol{i}^{L1}$ and $\boldsymbol{i}^{L2}$ are the branch currents and $\boldsymbol{i}^{L3}$ is the PCC-connected load current.

Voltage vectors of Bus-1 and Bus-3, that is $\boldsymbol{v}^{G1}$ and $\boldsymbol{v}^{G2}$, can be expressed as functions of the state variables of the lines, DG1 unit and DG2 unit, that is $\boldsymbol{i}^{L1}$, $\boldsymbol{i}^{L2}$, $\boldsymbol{i}_{G1}$ and $\boldsymbol{i}_{G2}$, respectively. The ODEs that represent these vectors are

$$\begin{aligned} \boldsymbol{v}^{G1} &= R_4(\boldsymbol{i}^{G1} - \boldsymbol{i}^{L1}) + L_4 \frac{\mathrm{d}}{\mathrm{d}t}(\boldsymbol{i}^{G1} - \boldsymbol{i}^{L1}) \\ \boldsymbol{v}^{G2} &= R_5(\boldsymbol{i}^{L2} - \boldsymbol{i}^{G2} - \boldsymbol{i}^{L6}) + L5 \frac{\mathrm{d}}{\mathrm{d}t}(\boldsymbol{i}^{L2} - \boldsymbol{i}^{G2} - \boldsymbol{i}^{L6}) \end{aligned} \tag{16}$$

where $\boldsymbol{i}^{L6}$ identifies the nonlinear part of the load connected to Bus-3 (Fig. 1).

Then, the network model in the micro-grid global $d-q$ reference frame of Fig. 3 is developed on the basis of the procedures outlined in Parniani [12] and given by

$$\Delta \dot{\boldsymbol{x}}_N = \boldsymbol{A}_N \Delta \boldsymbol{x}_N + \boldsymbol{B}_N^{v1}\Delta \boldsymbol{v}^{G1} + \boldsymbol{B}_N^{v2}\Delta \boldsymbol{v}^{G2} \tag{17}$$

and

$$\Delta \boldsymbol{v}^{G1} = \boldsymbol{E}_{11}^{N}\Delta \boldsymbol{x}_N + \boldsymbol{E}_{12}^{N}\Delta \dot{\boldsymbol{x}}_n + \boldsymbol{D}_{11}^{N}\Delta \boldsymbol{x}_{G1} + \boldsymbol{D}_{12}^{N}\Delta \dot{\boldsymbol{x}}_{G1} \tag{18}$$

$$\Delta \boldsymbol{v}^{G2} = \boldsymbol{E}_{21}^{N}\Delta \boldsymbol{x}_N + \boldsymbol{E}_{22}^{N}\Delta \dot{\boldsymbol{x}}_N + \boldsymbol{D}_{21}^{N}\Delta \boldsymbol{x}_{G2} + \boldsymbol{D}_{22}^{N}\Delta \dot{\boldsymbol{x}}_{G2} + \boldsymbol{B}^{N}\Delta \boldsymbol{u}_N \tag{19}$$

where

$$\Delta \boldsymbol{x}_N = \begin{bmatrix} \Delta \boldsymbol{i}_q^{L1} & \Delta \boldsymbol{i}_d^{L1} & \Delta \boldsymbol{i}_q^{L2} & \Delta \boldsymbol{i}_d^{L2} & \Delta \boldsymbol{i}_q^{L3} & \Delta \boldsymbol{i}_d^{L3} & \Delta \boldsymbol{v}_q^{\mathrm{pcc}} & \Delta \boldsymbol{v}_d^{\mathrm{pcc}} \end{bmatrix}^{\mathrm{T}}$$

$$\Delta \boldsymbol{u}_N = \begin{bmatrix} \Delta \boldsymbol{i}_q^{L6} & \Delta \boldsymbol{i}_d^{L6} \end{bmatrix}^{\mathrm{T}}.$$

The matrixes in (17–19) are defined in Katiraei [11].

4.4 Overall system model

Block diagram of Fig. 7 illustrates the input–output relations among the subsystems of the micro-grid, that is DG units and the network. on the basis of Fig. 7, the linearised models of DG1 and DG2, given by (8) and (13), respectively, are combined with the model of the network given by (17). The output current components of the DG units, represented by the vectors $\Delta \boldsymbol{i}^{G1}$ and $\Delta \boldsymbol{i}^{G2}$, are inputs

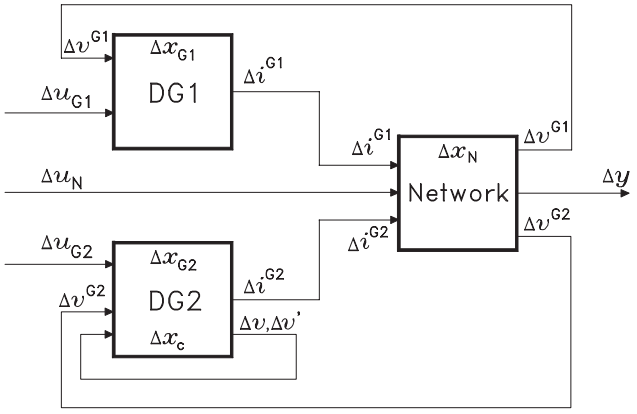

Fig. 7 *Block diagram of the system for developing state-space equations*

to the network system. Vectors of the bus voltages are considered as the output signals of the network model and inputs to DG1 and DG2.

The overall system state-space model is formulated in the form of (1), where

$$\Delta \boldsymbol{x} = [\Delta \boldsymbol{x}_{G1} \quad \Delta \boldsymbol{x}_{G2} \quad \Delta \boldsymbol{x}_N \quad \Delta \boldsymbol{x}_c]^{\mathrm{T}}$$

$$\Delta \boldsymbol{u} = [\Delta \boldsymbol{u}_{G1} \quad \Delta \boldsymbol{u}_{G2} \quad \Delta \boldsymbol{u}_N]^{\mathrm{T}}.$$

The system state matrix $\boldsymbol{A}$ and the coefficient matrix $\boldsymbol{B}$ of input signals are constructed from the coefficient matrices of the state-space models of the subsystems [11, 12].

5 Small-signal dynamic analysis

The linearised model of the system, that is (1), is used to investigate small-signal dynamic behaviour of the micro-grid system and design control parameters for the optimum performance. The linearised model is used for (i) eigenvalue analysis, (ii) frequency analysis through determination of the system transfer functions and (iii) step response analysis of the control systems. The small-signal model is also validated using a time-domain model of the system developed in the PSCAD/EMTDC environment.

5.1 Eigen analysis

Table 1 shows the eigenvalues of the system corresponding to an autonomous microgrid mode and a grid-connected mode of operation. The total steady-state power generation/consumption of the system, in the autonomous micro-grid mode, is given in Table 2. DG2 operates under voltage control mode and its terminal voltage is adjusted to 1.0 per unit. Terminal voltage of DG1 is also regulated at 1.0 per unit by its excitation system.

In the autonomous micro-grid mode, the system has nine pairs of complex–conjugate eigenvalues, Table 1. Eigenvalues 1–14 represent seven oscillatory modes, which correspond to the electrical interactions between (i) the DG units and (ii) the DG units and the network. For the given operating condition and the system parameters, these modes are highly damped. Eigenvalues 15 and 16 represent mechanical oscillatory mode of the rotor of DG1 with respect to the system. The frequency of this mode varies between 1 and 3 Hz depending on the operating point of the system. This oscillatory mode has a low damping, and Table 1 indicates that the damping is less in the autonomous micro-grid mode as compared with the grid-connected mode. Subsequent to an islanding process, this mode dominates the system dynamics.

Table 1: Eigenvalues of the micro-grid system

Eigen values	Grid-connected mode		Autonomous mode	
	Real (1/s)	Im (rad/s)	Real (1/s)	Im (rad/s)
1,2	—	—	−119.28	±2044.26
3,4	—	—	−147.06	±1293.26
5,6	−113.90	±486.80	−86.54	±675.74
7,8	−100.85	±436.19	−90.75	±430.86
9,10	−576.74	±376.93	−757.54	±376.41
11,12	−34.83	±372.13	−517.50	±371.09
13,14	−420.19	±376.98	−314.46	±364.13
15,16	−1.14	±23.17	−1.06	±10.41
17,18	−139.2, −138.4	0.0	−127.9	±8.42
19,20,21	−333.33	0.0	−333.33	0.0
22	−327.11	0.0	−326.18	0.0
23	−305.48	0.0	−137.46	0.0
24	−93.27	0.0	−93.04	0.0
25	−20.99	0.0	−24.39	0.0
26	−3.06	0.0	−17.26	0.0
27	−2.57	0.0	−2.57	0.0
28	−1.28	0.0	−0.672	0.0
29	−0.429	0.0	−0.277	0.0

Table 1 also shows that in the autonomous micro-grid mode, the system exhibits another oscillatory mode, which is represented by eigenvalues 17 and 18. The source of this oscillatory mode is the PLL of DG2 and is in response to the changes in the system frequency owing to the mechanical mode of DG1. Proper selection of the PLL parameters ensures that this mode is highly damped [17]. In the grid-connected mode, the eigenvalues associated with the PLL appear as two real eigenvalues, Table 1.

Fig. 8 shows loci of the eigenvalues of the mechanical mode of DG1 when the output power of DG2 is changed from 2.1 to 0.3 MW in steps of 0.6 MW, and for each amount of real power the ratio $k = Q_{DG2}/Q_{L3}$ is changed from 1.1 to 0.1. When $k = 0.1$, the reactive power of Load-3 is mostly supplied by the system, and when $k = 1.1$, DG2 supplies the reactive power of Load-3 and also dispatches reactive power to the network. Fig. 8 indicates that reducing real power decreases the damping of the mechanical mode.

Fig. 8 also shows that for a specified output real power of DG2, reducing the output reactive power of DG2 increases the damping of the mechanical mode of DG1. Fig. 8 reveals that the mechanical mode is highly damped when DG2 primarily injects real power in the system. This concludes that subsequent to disturbances, for example islanding, DG2 can

Table 2: Steady-state power generation/consumption in the autonomous micro-grid mode of operation (Fig. 2)

	Generation	Consumption
DG1	3.23 MW/0.28 MV	—
DG2	1.5 MVA/1.84 MVAr	—
Load 1	—	2.31 MW/1.49 MVAr
Load 2	—	0.6 MW/0.3 MVAr
Load 3	—	1.8 MW/1.82 MVAr
Capacitor C_p	1.5 MVAr	—

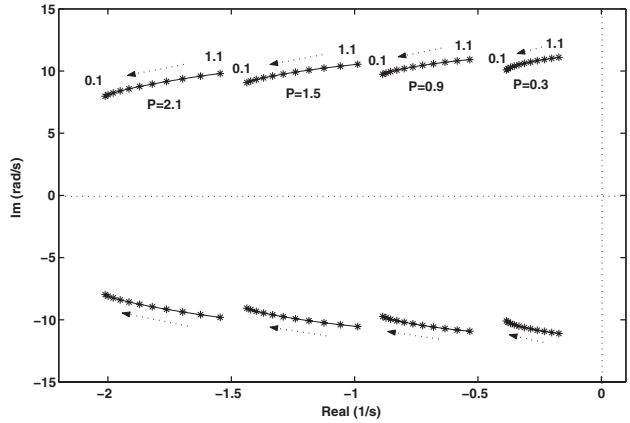

Fig. 8 *Loci of the eigenvalues of the mechanical mode of DG1 when real power of DG2 and $k = Q_{DG2}/Q_{L3}$ are changed*

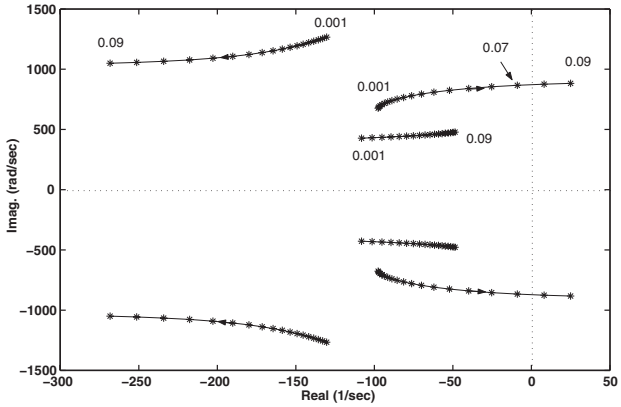

Fig. 10 *Loci of eigenvalues (3,4), (5,6) and (7,8) when K_p is changed from 0.001 to 0.09*

effectively mitigate the mechanical oscillations of DG1 through its real power control loop (Fig. 5*a*).

The eigen analysis approach is also used to perform sensitivity analysis and determine the ranges and/or optimum values of the control parameters for the micro-grid autonomous operation. Fig. 9 shows loci of conjugate pairs of eigenvalues (3,4) and (5,6) (Table 1) when the controller gain K_{pd}, that is the proportional gain of the real power controller of DG2 in Fig. 5*a*, assumes different values. Fig. 9 shows that the increasing K_{pd} from 0.001 to 0.2 results in departure of the pair of eigenvalue (3,4) from the left-hand plane to the right-hand plane (RHP). Thus, the corresponding oscillatory mode which is associated with the fixed-capacitor (Fig. 2) becomes unstable. In contrast, these changes of K_{pd} enhance the damping of the mode associated with the pair of eigenvalues (5,6).

Fig. 10 illustrates loci of eigenvalue pairs (3,4), (5,6) and (7,8) when the proportional gain K_p of the voltage control of DG2 in Fig. 5*a* is changed from 0.001 to 0.09. Fig. 10 indicates that the variations of K_p results in departure of eigenvalues (5,6) to the RHP. The other two modes remain stable, whereas changes in K_p reduce the damping of the mode associated with (7,8). On the basis of the results presented in Figs. 9 and 10, K_{pd} and K_p are selected at 0.1 and 0.01, respectively.

5.2 Step responses

Fig. 11 shows impact of 1% change of the voltage reference point v^{G2}_{rms} on Bus-3 voltage. The Bus-3 voltage is regulated

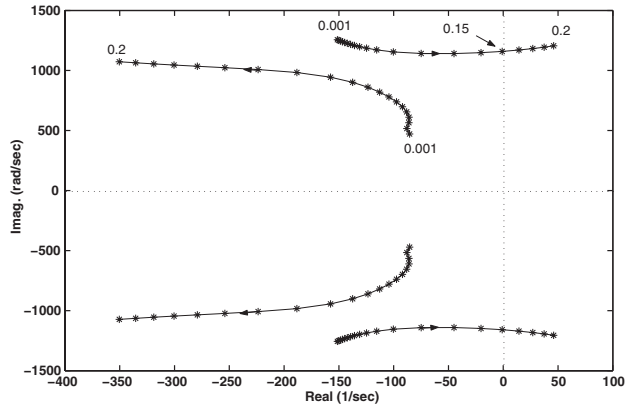

Fig. 9 *Loci of eigenvalues (3,4) and (5,6) when K_{pd} is changed from 0.001 to 0.2*

to the new set-point by injecting more reactive power into the system by an increase in the $q2$-axis current component of DG2 (Fig. 11*b*). Variations in the $d2$-axis current (Fig. 11*c*), is because of the coupling between the two controllers and also the changes in the reactive-power flow of the system as a result of an increase in Bus-3 voltage. Fig. 11 clearly shows the impact of the mechanical oscillatory mode of DG1 on the system response.

5.3 Validation of linear model

The PSCAD/EMTDC software package is used to develop the detail model of the system (Fig. 1) for time-domain simulation studies. Then, the results from the time-domain simulation studies have been compared with the corresponding results obtained from the linear model, for example Fig. 11, to establish the validity of the linear model. The operating point of the system is the same as given in Table 2.

Fig. 12 shows the system response, on the basis of the PSCAD/EMTDC model, to 1% increase in the voltage set-point of Bus-3. The voltage increase requires that DG2 needs to inject more reactive power by increasing the

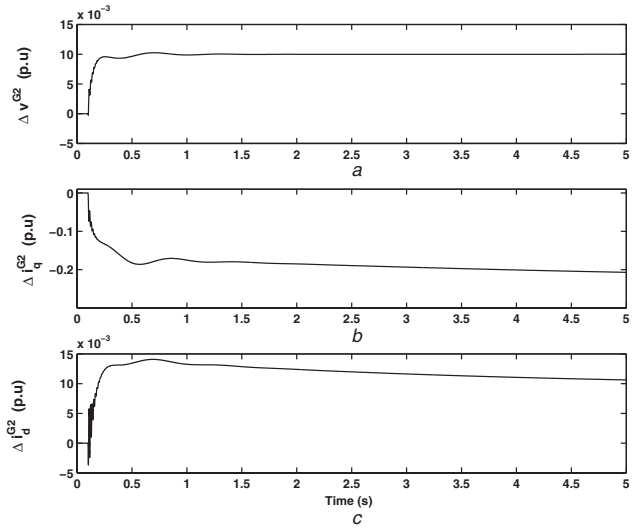

Fig. 11 *System response to 1% step change in rms value of Bus-3 voltage Δv^{G2}_{rms}, in the autonomous mode (linearised model)*

a Bus-3 voltage
b $q2$-axis current
c $d2$-axis current

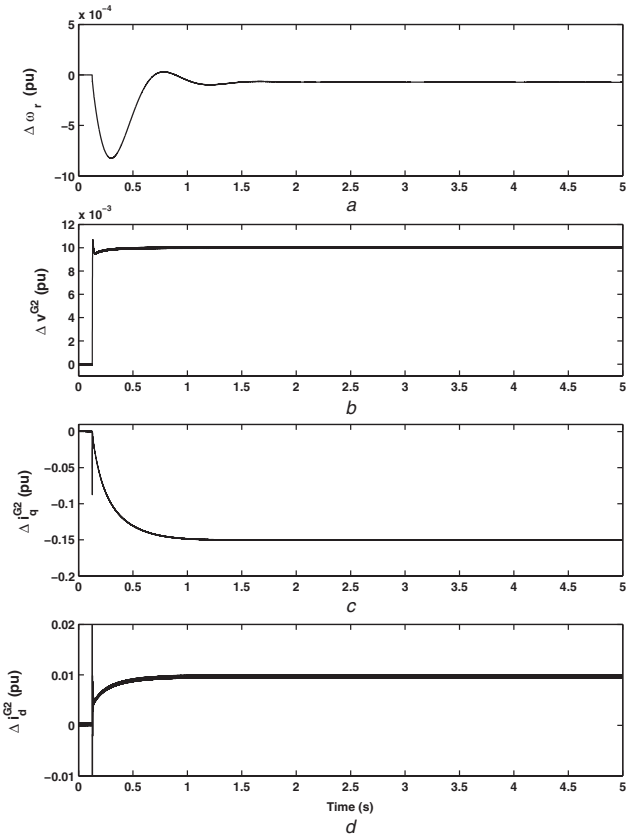

Fig. 12 *System responses to 1% step change in the voltage of Bus-3 v_{rms}^{G2} (PSCAD/EMTDC results)*

a DG1 speed
b Bus-3 voltage
c *q*2-axis current
d *d*2-axis current

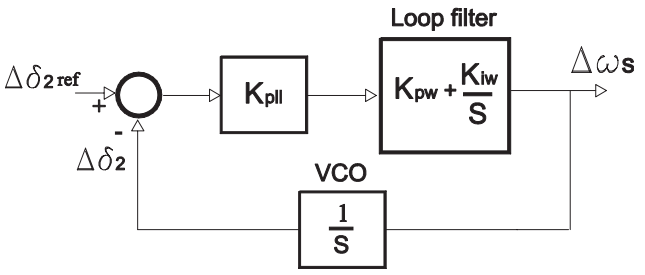

Fig. 13 *Linearised model of the PLL of DG2*

*q*2-axis current component (Fig. 12*c*). The increase in the Bus-3 voltage changes the reactive-power balance of the system which leads to the deviations in the DG1 speed (Fig. 12*a*) and slight reduction in the real power of DG2. The real-power reduction is accommodated by a decrease in the *d*2-axis current component of DG2, Fig. 12*d*. Comparison of the simulation results of Fig. 12 with the corresponding results from the linear model, that is Fig. 11, qualitatively verify the validity of the linear model and the accuracy of the results.

Comparing the simulation results demonstrated in Fig. 12 with those of Fig. 11, respectively, indicates (i) similar patterns of behaviour of the system variables, (ii) approximately identical settling points and (iii) comparable time-constant and over-shoot values associated with the corresponding system responses. The PSCAD/EMTDC results with system responses are slightly different from the small-signal analysis owing to the difference in the method of implementation and the time delays applied by measurement/calculation blocks. The system responses from the nonlinear model are highly dependent on the point-on-wave disturbance and dynamics of measurement and actuator devices that cannot be accommodated in the small-signal model.

6 Conclusions

This paper presents a small-signal dynamic model of a micro-grid system in a rotating *dq*0 frame. The DG units of the micro-grid comprise a synchronous generator and an electronically interfaced DG unit. The paper also describes and formulates the controllers of the DG units. The control strategies for various modes of operation of the micro-grid are also presented. The mathematical process and structure for the development of micro-grid model are presented in a general form and can be expanded to include additional DG units, loads and controllers as desired. The developed model captures frequency deviation of the autonomous micro-grid and includes the PLL model to dynamically synchronise the electronically interfaced DG unit with the network frequency. Frequency restoration is carried out by the governor of the synchronous machine.

Applications of the model to (i) investigate dynamics of the micro-grid and (ii) design/optimise controllers of the electronically interfaced DG unit during grid-connected and islanded modes of operation are presented. These studies show that the fast control action of the electronically interfaced DG unit can be exploited to meet changes in power demand, maintain angle/voltage stability and enhance voltage quality during the grid-connected and the autonomous micro-grid modes of operation. The study results of the linearised model have been qualitatively validated on the basis of the comparison with the results from time-domain simulation of the micro-grid in the PSCAD/EMTDC software environment.

7 References

1 Davis, M.W.: 'Distributed resource electric power systems offer significant advantages over central station generation and T&D Power Systems, Part I'. IEEE T&D Conf. Exposition, Atlanta, Gorgia, October/November 2001, pp. 54–61
2 Davis, M.W., Gifford, A.H., and Krupa, T.J.: 'Microturbines-an economic and reliability evaluation for commercial, residential, and remote load applications', *Power Syst. IEEE Trans. Power Syst.*, 1999, **14**, (4), pp. 1556–1562
3 Hatziargyriou, N.D., and Sakis Meliopoulos, A.P.: 'Distributed energy sources: technical challenges'. Proc. IEEE PES Winter Meeting, 2002, New York, vol. 2, pp. 1017–1022
4 Smallwood, C.L.: 'Distributed generation in autonomous and non-autonomous micro grids'. Proc. Rural Electric Power Conf., IEEE, May 2002, pp. D1/1–D1/6
5 Piagi, P., and Lasseter, R.H.: 'Industrial application of mirogrids'. Technical Report, Power System Engineering Research Center, University of Wisconsin-Madison, October 2001
6 Katiraei, F., Iravani, M.R., and Lehn, P.W.: 'Micro-grid autonomous operation during and subsequent to islanding process', *IEEE Trans. Power Deliv.*, 2005, **20**, (1), pp. 248–257
7 IEEE WG: 'IEEE standard for interconnecting distributed resources with electric power systems'. IEEE Std 1547-2003, IEEE Publication, July 2003
8 Chandorkar, M.C., Divan, D.M., and Banerjee, B.: 'Control of distributed UPS systems'. Power Electronics Specialists Conf., PESC '94 Record., 25th Annual IEEE, June 1994, vol. 1, pp. 197–204
9 Schauder, C., and Mehta, H.: 'Vector analysis and control of the advanced static VAR compensators'. IEE Proc.-C, July 1993, vol. 140, 4, pp. 299–306
10 Krause, P.C.: 'Analysis of electric machinery and drive systems' (IEEE Press, 2002)

11 Katiraei, F.: 'Dynamic analysis and control of distributed energy resources in a micro-grid'. PhD dissertation, University of Toronto, Toronto-Ontario, July 2005
12 Parniani, M., and Iravani, M.R.: 'Computer analysis of small-signal stability of power systems including network dynamics', *IEE Proc.*, 1995, **142**, (6), pp. 613–617
13 Undrill, J.M.: 'Dynamic stability calculations for an arbitrary number of interconnected synchronous machines', *IEEE Trans. Power Appl. Syst.*, 1968, **PAS-87**, pp. 835–844
14 IEEE WG: 'IEEE recommended practice for excitation system models for power system stability studies'. IEEE Std 421.5-1992
15 Working Group on Prime Mover and Energy Supply Models for System Dynamic Performance Studies: 'Dynamic models for fossil fueled steam units on power system studies', *IEEE Trans. Power Sys.*, 1991, **6**, (2), pp. 753–761
16 Chung, S.K.: 'A phase tracking system for three phase utility interface inverters', *IEEE Trans. PE*, 2000, **15**, (3), pp. 431–438
17 Coelho, E.A.A., Cortiz, P.C., and Garcia, P.F.D.: 'Small-signal stability for parallel-connected inverters in stand-alone AC supply systems', *IEEE Trans. Ind. Appl.*, 2002, **38**, (2), pp. 533–542

8 Appendix A

The state-space model of the DG2 controller represents the PI controllers, the low-pass filter, and the PLL, Figs. 5 and 6. The model of the PI controller is

$$\begin{aligned} \Delta \dot{\boldsymbol{x}}_i &= \Delta \boldsymbol{x}_{\text{ref}} - \Delta \boldsymbol{x} \\ \Delta \boldsymbol{x}_{\text{out}} &= K_i \Delta \boldsymbol{x}_i + K_p(\Delta \boldsymbol{x}_{\text{ref}} - \Delta \boldsymbol{x}) \end{aligned} \tag{20}$$

where K_p and K_i are the proportional and the integral gains. $\Delta \boldsymbol{x}$ is passed through a first-order low-pass filter with the time-constant of τ_i to provide $\Delta \boldsymbol{x}_f$

$$\Delta \dot{\boldsymbol{x}}_f = \frac{1}{\tau_i}\Delta \boldsymbol{x} - \frac{1}{\tau_i}\Delta \boldsymbol{x}_f \tag{21}$$

Fig. 13 shows the linearised model of the PLL. The mathematical representation of the PLL is

$$\Delta \dot{\boldsymbol{\omega}}_s = -K_{\text{pll}} K_{pw} \Delta \boldsymbol{\omega}_s - K_{\text{pll}} K_{iw}(\Delta \boldsymbol{\delta}_2(\text{ref}) - \Delta \boldsymbol{\delta}_2) \tag{22}$$

where K_{pll} is the gain factor representing the monitoring and sampling stage, and K_{pw} and K_{iw} are proportional and integral gains of the loop filter, respectively [16]. In (22), $\Delta \boldsymbol{\delta}_2$ (ref) is the phase angle of the input signal to the PLL that represents the reference angle for tracking [16].